RESEARCH MEMORANDUM

WIND-TUNNEL INVESTIGATION OF HORIZONTAL TAILS. V - 45° SWEPT-BACK PLAN FORM OF ASPECT RATIO 2

By Jules B. Dods, Jr.

Ames Aeronautical Laboratory
Moffett Field, Calif.

NATIONAL ADVISORY COMMITTEE
FOR AERONAUTICS

WASHINGTON
September 27, 1949

NATIONAL ADVISORY COMMITTEE FOR AERONAUTICS

RESEARCH MEMORANDUM

WIND-TUNNEL INVESTIGATION OF HORIZONTAL TAILS. V - 45° SWEPT-BACK PLAN FORM OF ASPECT RATIO 2

By Jules B. Dods, Jr.

SUMMARY

The results of a wind-tunnel investigation of the low-speed aerodynamic characteristics of a 45° swept-back horizontal-tail model of aspect ratio 2 are presented, and are compared with previous results for a model of the same aspect ratio having an unswept hinge line. These data supplement previously reported results of tests of models having unswept hinge lines and models having the 0.25-chord line swept back 35° with aspect ratios of 3, 4.5, and 6.

Test results are presented for the 45° swept-back model with and without standard roughness on the leading edge, with a sealed radius-nose elevator, and with an unsealed radius-nose elevator. The test Reynolds numbers varied from 3.0 to 7.5 million. The tests included measurement of the model lift and pitching moment, of the elevator hinge moment, and of the pressure difference across the elevator nose seal. Tuft studies of the air flow over the model with the elevator undeflected and with it deflected are presented.

The major effects of sweepback, as measured in the low-speed tests of the models of aspect ratio 2, were to increase the negative rate of change of hinge-moment coefficient with angle of attack, to reduce the negative rate of change of hinge-moment coefficient with elevator deflection, and to reduce the elevator-effectiveness parameter. Sweepback also reduced the static longitudinal stability.

INTRODUCTION

A systematic investigation of the control-surface characteristics, particularly the hinge-moment parameters, of horizontal-tail surfaces has been undertaken by the NACA to provide design data and experimental

results for comparison with the parameters estimated by the lifting-surface theory.

Experimental results from wind-tunnel tests of models having unswept hinge lines and models having the 0.25-chord lines swept back 35° and having aspect ratios of 3, 4.5, and 6 are presented in reference 1, parts I, II, and III. In addition, experimental results have been presented in reference 1, part IV, for a model of aspect ratio 2 having an unswept hinge line and for a two-dimensional model with the NACA 64A010 section which was common to all the models. The purpose of the present report is to provide experimental data for a 45° swept-back model of aspect ratio 2 for design use and for comparison with the results of the model with the unswept hinge line having an aspect ratio of 2. The angle of sweepback for the present model was 45°, instead of the 35° used for other swept models of the series, because the greater sweepback was believed to result in a more acceptable plan form for the aspect ratio of 2.

NOTATION

Coefficients

C_{h_e} elevator hinge-moment coefficient ($H/qS_e\bar{c}_e$) (See appendix.)

C_L lift coefficient (L/qS)

C_m pitching-moment coefficient ($M/qS\bar{c}$)

$\Delta p/q$ pressure coefficient across elevator nose seal $\left(\frac{\text{pressure below seal} - \text{pressure above seal}}{\text{free-stream dynamic pressure}}\right)$

Symbols

A aspect ratio ($2b^2/S$)

b span of the semispan model measured perpendicular to the plane of symmetry, feet

b_e' span of the elevator of the semispan model measured along the hinge line, feet

c chord of the model measured parallel to the plane of symmetry, feet

$\bar{c}$ mean aerodynamic chord $\left(\frac{\int_0^b c^2 dy}{\int_0^b c\, dy}\right)$, feet

c_e chord of the elevator behind the hinge line, measured parallel to the plane of symmetry, feet

c_e' chord of the elevator behind the hinge line, measured perpendicular to the hinge line, feet

$\bar{c}_e$ root-mean-square chord of the elevator behind the hinge line, measured parallel to the plane of symmetry, feet

$\bar{c}_e'$ root-mean-square chord of the elevator behind the hinge line, measured perpendicular to the hinge line, feet

H hinge moment, foot-pounds

L lift, pounds

M pitching moment about a lateral axis through a point at 0.25 of the mean aerodynamic chord, foot-pounds

M_A first moment of the elevator area behind the hinge line about the hinge line, feet cubed

q free-stream dynamic pressure $\left(\frac{1}{2}\rho V^2\right)$, pounds per square foot

R Reynolds number $(\rho V\bar{c}/\mu)$

S area of semispan model, square feet

S_e area of the elevator of the semispan model behind the hinge line, square feet

t thickness of model in plane of symmetry, feet

V velocity of air, feet per second

y lateral distance, feet

α corrected angle of attack, degrees

δ_e elevator deflection (positive when trailing edge of elevator is down) measured in a plane normal to the hinge line, degrees

μ absolute viscosity, slugs per foot-second

ρ density of air, slugs per cubic foot

Parameters

$C_{h_\alpha} = \left(\frac{\partial C_{h_e}}{\partial \alpha}\right)_{\delta_e = 0}$ (measured through $\alpha = 0$)

$C_{h_{\delta_e}} = \left(\frac{\partial C_{h_e}}{\partial \delta_e}\right)_{\alpha = 0}$ (measured through $\delta_e = 0$)

$C_{L_\alpha} = \left(\frac{\partial C_L}{\partial \alpha}\right)_{\delta_e = 0}$ (measured through $\alpha = 0$)

$C_{L_{\delta_e}} = \left(\frac{\partial C_L}{\partial \delta_e}\right)_{\alpha = 0}$ (measured through $\delta_e = 0$)

$\alpha_{\delta_e} = -\frac{C_{L_{\delta_e}}}{C_{L_\alpha}}$ elevator-effectiveness parameter

MODEL

The semispan, or reflection-plane, model used in this investigation had an aspect ratio of 2 and a taper ratio (ratio of tip chord to root chord) of 0.5. The 0.25-chord line was swept back 45°, as shown in figure 1. The model had the NACA 64A010 airfoil section perpendicular to the 0.25-chord line. The section coordinates are given in table I. This section was the same as that of the models used in the tests reported in reference 1.

The model was equipped with a sealed radius-nose elevator having a chord equal to 0.30 of the airfoil chord perpendicular to the 0.25-chord line. The ratio of elevator area to total surface area was 0.231.

The gap between the elevator and the shrouds, and the gap between the elevator nose and the balance plate (seal gap) are shown in figure 1. The elevator nose gap was sealed from the root to the tip. The pressure orifices in the balance chamber enclosed by the shrouds were

located both above and below the seal at four spanwise stations. The ends of the balance chamber were sealed at the root and at the outer hinge bracket. One elevator hinge bracket was immediately below the tunnel floor, and the other bracket was at 82 percent of the span. The balance-chamber pressure orifices at 91-percent span were, therefore, outboard of the hinge brackets.

The tip shape was formed by rotating the airfoil section parallel to the undisturbed air stream about a line which was inboard of the tip a distance equal to one-half of the maximum thickness of the tip.

Photographs of the model mounted in the wind tunnel are shown in figure 2.

TESTS

The tests were conducted in one of the Ames 7- by 10-foot wind tunnels. The model was mounted on a turntable flush with the tunnel floor (fig. 2), and was tested with a dynamic pressure of 28 pounds per square foot, corresponding to a Reynolds number of 3.0 million. A limited amount of data was also obtained at Reynolds numbers of 4.0, 5.0, and 7.5 million. Unless otherwise specified, the model was smooth and the elevator was sealed. For those tests with leading-edge roughness, the elevator was sealed; the tests with the elevator nose seal removed were made with a smooth leading edge. The leading-edge roughness was applied as described in reference 2 for standard roughness. The studies of the air flow over the model, as indicated by short tufts of thread, were made at a Reynolds number of 3.0 million.

The lift and pitching moment of the model were measured by means of the wind-tunnel balance system. The elevator hinge moment was measured by means of a resistance-type torsional strain gage. Pressures above and below the elevator nose seal in the balance chamber were measured by the use of a manometer connected to the orifices in the balance chamber.

CORRECTIONS

All coefficients and the angle of attack have been corrected for the effects of the tunnel walls by the methods of reference 3. The data were corrected as follows:

$$\alpha = \alpha_u + 0.934\ C_{L_u} + 0.174\ C_{L_{u(\delta_e = 0)}}$$

$$C_m = C_{m_u} + 0.00499\, C_{L_u}$$

$$C_{h_e} = C_{h_{e_u}} + 0.00678\, C_{L_u}$$

$$C_L = 0.993\, C_{L_u}$$

where the subscript u refers to the uncorrected coefficient or angle of attack.

RESULTS AND DISCUSSION

The results of tests of the 45° swept-back model of aspect ratio 2 are presented in figures 3 to 10. The variations of lift, hinge-moment, and pitching-moment coefficients with angle of attack for various elevator deflections are given in figure 3. Hinge-moment coefficients are also shown as a function of the elevator deflection for various angles of attack in figure 4. The variation of the pressure coefficient across the elevator nose seal with angle of attack is presented in figure 5. Effects of the variation of the Reynolds number, of the standard roughness, and of the elevator nose seal on the lift and hinge-moment coefficients are shown in figures 6 to 8. Tuft studies of the air flow over the model are shown in figures 9 and 10 with the elevator undeflected and with it deflected up 15°, respectively.

In the following discussion the results of the present tests are compared with those of reference 1, part IV, for a model having the same aspect ratio and taper ratio, but with the hinge line unswept. The model with the unswept hinge line will hereinafter be referred to as the unswept model. The unswept model had a small amount of sweepback of the 0.25-chord line (16.7°), which was the result of following normal design practice for tails having the control-surface hinge line in a plane perpendicular to the plane of symmetry. The sweep reference line for the 45° swept-back model was the line joining the 0.25-chord points of the NACA 64A010 airfoil sections which were inclined at an angle of 45° to the plane of symmetry. This reference line corresponded to a line through the 0.323-chord points of sections in planes parallel to the plane of symmetry. The airfoil profiles and the elevator-chord ratios in planes perpendicular to the sweep reference line of the swept-back model were identical to the profiles and elevator-chord ratios in planes parallel to the plane of symmetry for the unswept model. This correspondence facilitates a comparison of the experimental results with theoretical results involving aspect-ratio corrections for section lift and hinge-moment parameters. The geometric characteristics of the unswept and swept-back models are different in planes parallel to the plane of symmetry, as shown by the following table:

Model	Elevator-chord ratio, $\frac{c_e}{c}$	Thickness ratio, $\frac{t}{c}$	Trailing-Edge angle (deg)
Unswept	0.30	0.100	12
Swept back	.23	.079	8

According to the usual convention, the elevator deflections for both models were measured in planes perpendicular to the elevator hinge line.

Lift and Hinge-Moment Parameters

The lift and the hinge-moment parameters are listed in table II[1] for both the unswept model and the 45° swept-back model. As shown by this table, C_{h_α} changed from -0.0002 for the unswept model to -0.0013 for the swept-back model; the change in $C_{h_{\delta_e}}$ was from -0.0072 to -0.0057; and the elevator-effectiveness parameter α_{δ_e} was changed from -0.73 to -0.51. The value of $C_{L_{\delta_e}}$ was reduced from 0.029 to 0.021, but C_{L_α} was practically unchanged.

Static Longitudinal Stability

The variation of pitching-moment coefficient with angle of attack for the unswept and the swept-back models indicated a destabilizing effect of sweepback; the aerodynamic center was shifted forward about 2 percent of the mean aerodynamic chord. Both models were statically unstable at small angles of attack as evidenced by a value of $(dC_m/d\alpha)_{\delta_e = 0}$ of 0.0023 for the unswept model and a value of 0.0031 for the swept-back model.

The experimental results which indicate a destabilizing effect of sweepback for the models of aspect ratio 2 and a stabilizing effect of sweepback for the models of aspect ratios of 3, 4.5, and 6 are not in exact agreement with the theoretical results shown in figure 4 of reference 4. The theoretical results indicate two effects: (1) a stabilizing effect of increasing the sweepback for a constant aspect

[1]The values of the lift and hinge-moment parameters were derived from large-scale plots of the data.

ratio, and (2) a destabilizing effect of reducing the aspect ratio for a constant angle of sweepback. The combination of these two theoretical effects results in no change in stability between a model of aspect ratio 3 swept back 35° and a model of aspect ratio 2 swept back 45°. Experimentally, however, there was a destabilizing shift in the aerodynamic center of about 4 percent between these models.

The results of a statistical analysis of a group of plan forms of various aspect ratios and angles of sweepback presented in reference 5 indicate that the static longitudinal stability at the stall decreases with increasing sweepback. The experimental results are in agreement with this reference, since they indicate a decided increase in the static longitudinal stability at the stall for the unswept model but only a slight increase in the stability for the swept-back model. (See fig. 3(c) and reference 1, part IV, fig. 4(c).)

Effect of Reynolds Number

The effects of variation of the Reynolds number from 3.0 to 7.5 million are shown in figure 6 for the swept-back model. The maximum lift characteristics of the model were relatively unaffected by this variation of Reynolds number, but a small reduction in $C_{L_{\delta_e}}$ was noted (as measured through zero angle of attack). The value of C_{h_α} remained nearly constant with increasing Reynolds number, but there was a small increase in $C_{h_{\delta_e}}$.

The maximum lift coefficient of the unswept model (reference 1, part IV) increased slightly with increasing Reynolds number, but there was no change in the lift or hinge-moment parameters corresponding to small lift coefficients.

Effect of Standard Roughness

The effects of standard leading-edge roughness upon the lift and hinge-moment coefficients with the elevator nose gap sealed are shown in figure 7 for the swept-back model of aspect ratio 2. As shown in this figure, and in table II, there was no change in C_{L_α}, $C_{L_{\delta_e}}$, or C_{h_α}, but there was a reduction in the negative value of $C_{h_{\delta_e}}$ from -0.0057 to -0.0055. At the larger elevator deflections, the effect of roughness was to reduce the hinge moments slightly at the smaller angles of attack.

For the unswept model a similar reduction in $C_{h_{\delta_e}}$ was measured, and, in addition, the value of C_{h_α} was changed from -0.0002 to 0.0006.

Effect of Removing Elevator Nose Seal

The major effect of removing the elevator nose seal (models smooth) was to reduce the elevator lift-effectiveness parameter $C_{L_{\delta_e}}$ of the swept-back model with a consequent reduction of α_{δ_e}. As shown in figure 8 and table II, $C_{L_{\delta_e}}$ was reduced from 0.021 to 0.018. The lift-curve slope C_{L_α} remained constant. A small change in C_{h_α} and $C_{h_{\delta_e}}$ was also measured.

The only noteworthy effects upon the characteristics of the unswept model were to change $C_{h_{\delta_e}}$ from -0.0072 to -0.0074 and to reduce the maximum lift coefficient.

Visualization of the Air Flow

The photographic studies of the air flow as indicated by tufts on the upper and lower surfaces of the swept-back model with the elevator undeflected and deflected up 15° are presented in figures 9 and 10, respectively.

With the elevator undeflected, and with the model at an angle of attack of 0° (figs. 9(a) and 9(b)), the air flow over both the upper and lower surfaces was smooth. At an angle of attack of 4.2° (figs. 9(c) and 9(d)) a noticeable outward flow had started over the elevator, and at the tip of the model the tufts indicated a flow from the lower to the upper surface. The front spanwise row of tufts on the lower surface also showed a tendency for the air to flow outward. At an angle of attack of 12.6° (figs. 9(e) and 9(f)) rough flow at the tip was evidenced. Separation apparently began near the leading edge; this fact has also been indicated by liquid-film studies. Further increases in the angle of attack caused the area of rough flow to progress inward. Figures 9(k) and 9(l) illustrate the conditions existing just below the angle of attack for the maximum lift coefficient, which was approximately 27°, and figures 9(m) to 9(p) illustrate the conditions at the stall.

The studies of the tufts on the model with the elevator deflected up 15°, presented in figure 10, show that the rough flow again started at the tip and progressed inward. The maximum lift coefficient occurred at about the same angle of attack as it did with the elevator undeflected (fig. 3(a)). An interesting feature of the tuft studies of the model with the elevator deflected was the reduction in the outward flow along the lower surface of the elevator as the elevator became more closely alined with the undisturbed air stream at the larger angles of attack.

CONCLUSIONS

The results of tests conducted to evaluate the low-speed aerodynamic characteristics of a 45° swept-back tail model of aspect ratio 2, when compared with the results of previous tests of a model of the same aspect ratio with the hinge line unswept, indicated that:

1. The value of C_{h_α} was changed from −0.0002 for the unswept model to −0.0013 for the 45° swept-back model.

2. The value of $C_{h_{\delta_e}}$ was changed from −0.0072 for the unswept model to −0.0057 for the 45° swept-back model.

3. The elevator-effectiveness parameter α_{δ_e} was changed from −0.73 for the unswept model to −0.51 for the 45° swept-back model.

4. Sweepback reduced the static longitudinal stability as shown by a forward shift of the aerodynamic center of about 2 percent of the mean aerodynamic chord.

5. The effect of increasing Reynolds number was to reduce $C_{L_{\delta_e}}$ and to increase $C_{h_{\delta_e}}$ for the swept-back model. No significant scale effects had been encountered for the unswept model.

6. The effect of standard leading-edge roughness on the unswept model had been to change C_{h_α} from −0.0002 to 0.0006. There was no change in C_{h_α} for the swept-back model with roughness.

7. The major effect of removing the elevator nose seal was to reduce the elevator lift-effectiveness parameter $C_{L_{\delta_e}}$ of the swept-back model.

Ames Aeronautical Laboratory,
National Advisory Committee for Aeronautics,
Moffett Field, Calif.

APPENDIX

CONVERSION FACTORS FOR HINGE-MOMENT COEFFICIENTS

Because several methods are in use for the conversion of hinge moments to nondimensional coefficients, particularly for swept-back lifting surfaces, factors relating the various methods are presented. To obtain the hinge-moment coefficients for one of the listed methods, multiply the value of the hinge-moment coefficients of this report by the corresponding factor in the following table:

Equations for hinge-moment coefficients	45° swept-back model of aspect ratio 2	
	H/qC_{h_e} (ft^3)	Conversion factor
$C_{h_e} = \frac{H}{qS_e\bar{c}_e}$	1.734	1.000
$C_{h_e} = \frac{H}{qb\bar{c}_e^2}$	1.767	0.981
$C_{h_e} = \frac{H}{qb_e'(\bar{c}_e')^2}$	1.444	1.201
$C_{h_e} = \frac{H}{2qM_A}$	1.444	1.201

REFERENCES

1. Dods, Jules B., Jr.: Wind-Tunnel Investigation of Horizontal Tails.

I- Unswept and 35° Swept-Back Plan Forms of Aspect Ratio 3. NACA RM A7K24, 1948.

II- Unswept and 35° Swept-Back Plan Forms of Aspect Ratio 4.5. NACA RM A8B11, 1948.

III– Unswept and 35° Swept-Back Plan Forms of Aspect Ratio 6. NACA RM A8H30, 1948.

IV– Unswept Plan Form of Aspect Ratio 2 and a Two-Dimensional Model. NACA RM A8J21, 1948.

2. Abbott, Ira H., von Doenhoff, Albert E., and Stivers, Louis S., Jr.: Summary of Airfoil Data. NACA Rep. 824, 1945.

3. Swanson, Robert S., and Toll, Thomas A.: Jet-Boundary Corrections for Reflection-Plane Models in Rectangular Wind Tunnels. NACA Rep. 770, 1943.

4. DeYoung, John: Theoretical Additional Span Loading Characteristics of Wings with Arbitrary Sweep, Aspect Ratio, and Taper Ratio. NACA TN 1491, 1947.

5. Shortal, Joseph A., and Maggin, Bernard: Effect of Sweepback and Aspect Ratio on Longitudinal Stability Characteristics of Wings at Low Speeds. NACA TN 1093, 1946.

TABLE I.— COORDINATES FOR THE NACA 64A010 AIRFOIL AND THE MODEL TESTED

[All Dimensions in Percent of Wing Chord]

Upper and Lower Surfaces		
Station	NACA 64A010 ordinate	Model ordinate
0	0	0
.50	.804	.819
.75	.969	.987
1.25	1.225	1.247
2.50	1.688	1.696
5.00	2.327	2.333
7.50	2.805	2.780
10.00	3.199	3.202
15.00	3.813	3.816
20.00	4.272	4.280
25.00	4.606	4.610
30.00	4.837	4.842
35.00	4.968	4.950
40.00	4.995	4.975
45.00	4.894	4.889
50.00	4.684	4.672
55.00	4.388	4.373
60.00	4.021	4.011
65.00	3.597	3.594
70.00	3.127	3.131
75.00	2.623	2.637
80.00	2.103	2.120
85.00	1.582	1.595
90.00	1.062	1.071
95.00	.541	.553
100.00	.021	.022
L. E. Radius 0.687[a]; T. E. Radius 0.023[a]		

[a]Same for both the NACA 64A010 section and the model.

TABLE II.- A SUMMARY OF THE LIFT AND HINGE-MOMENT PARAMETERS OF THE UNSWEPT AND THE 45° SWEPT-BACK MODELS OF ASPECT RATIO 2 (R, 3.0×10^6)

Parameter	Model Condition		
	Model smooth; elevator sealed	Model with standard roughness; elevator sealed	Model smooth; elevator seal removed
Unswept[a]			
C_{h_α}	−0.0002	0.0006	−0.0002
$C_{h_{\delta_e}}$	−.0072	−.0070	−.0074
C_{L_α}	.040	.040	.040
$C_{L_{\delta_e}}$	.029	.029	.029
α_{δ_e}	−.73	−.73	−.73
Swept back			
C_{h_α}	−0.0013	−0.0013	−0.0012
$C_{h_{\delta_e}}$	−.0057	−.0055	−.0054
C_{L_α}	.041	.041	.041
$C_{L_{\delta_e}}$	.021	.021	.018
α_{δ_e}	−.51	−.51	−.44

[a]Parameters for the unswept model are from reference 1, part IV.

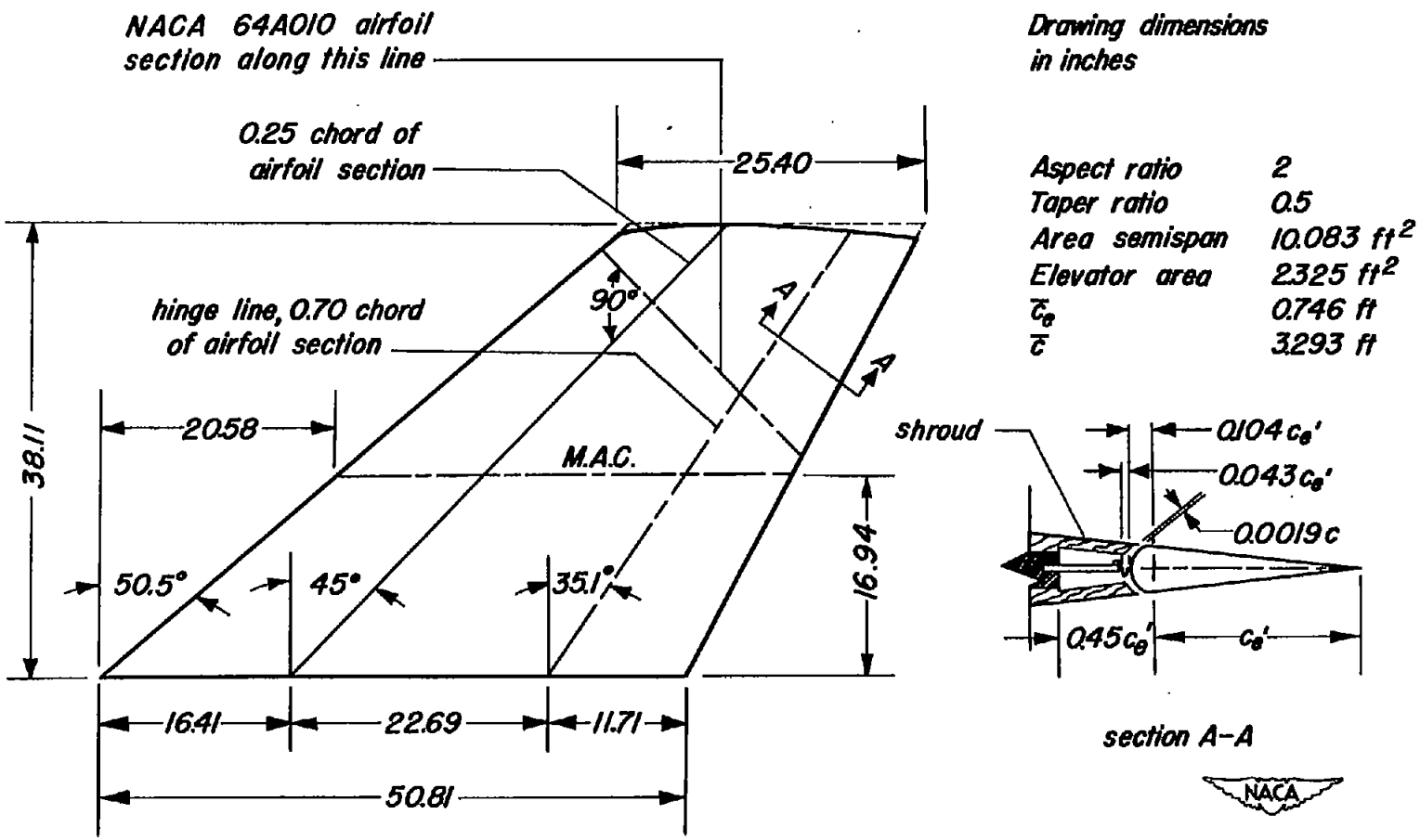

Figure 1.-The 45° swept-back horizontal tail model of aspect ratio 2.

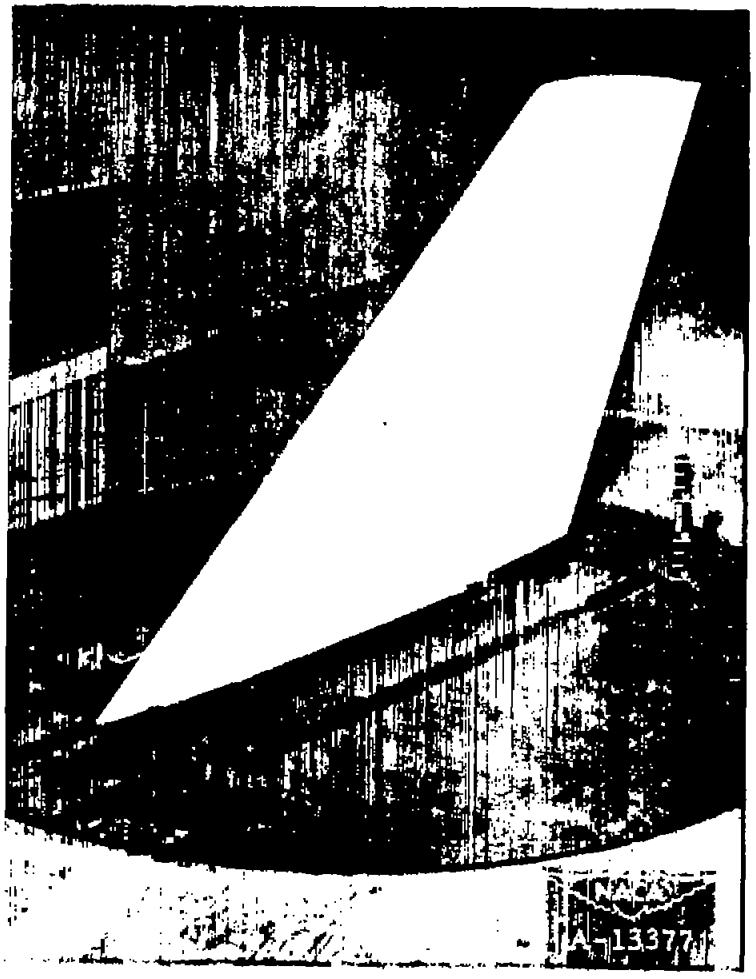

(a) Three-quarter front view.

(b) Three-quarter rear view.

Figure 2.– The 45° swept-back model of aspect ratio 2 mounted in the Ames 7- by 10-foot wind tunnel.

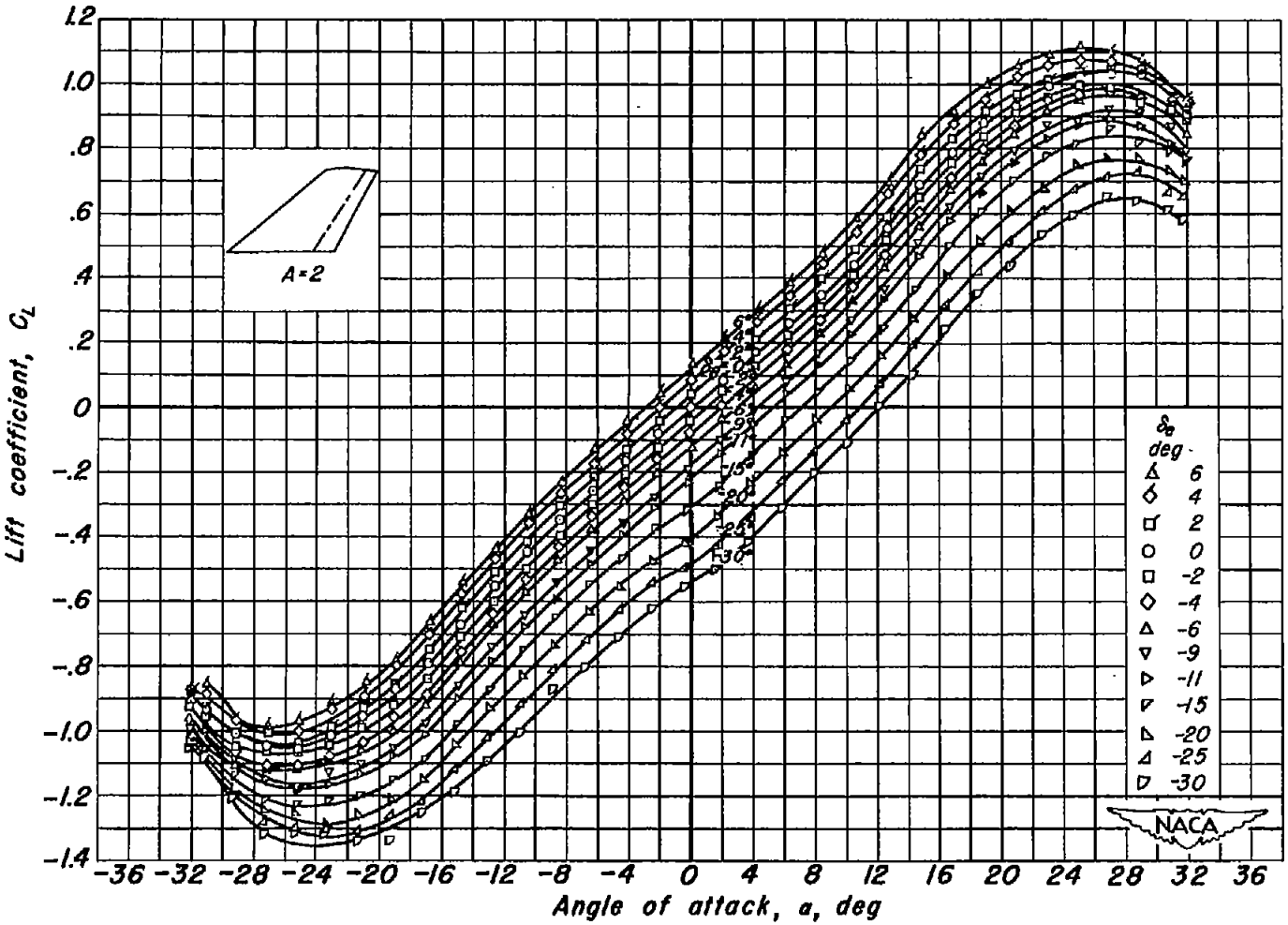

(a) Lift coefficient.

Figure 3.– Lift, hinge-moment, and pitching-moment coefficients for the 45° swept-back model of aspect ratio 2. R, 3.0×10^6.

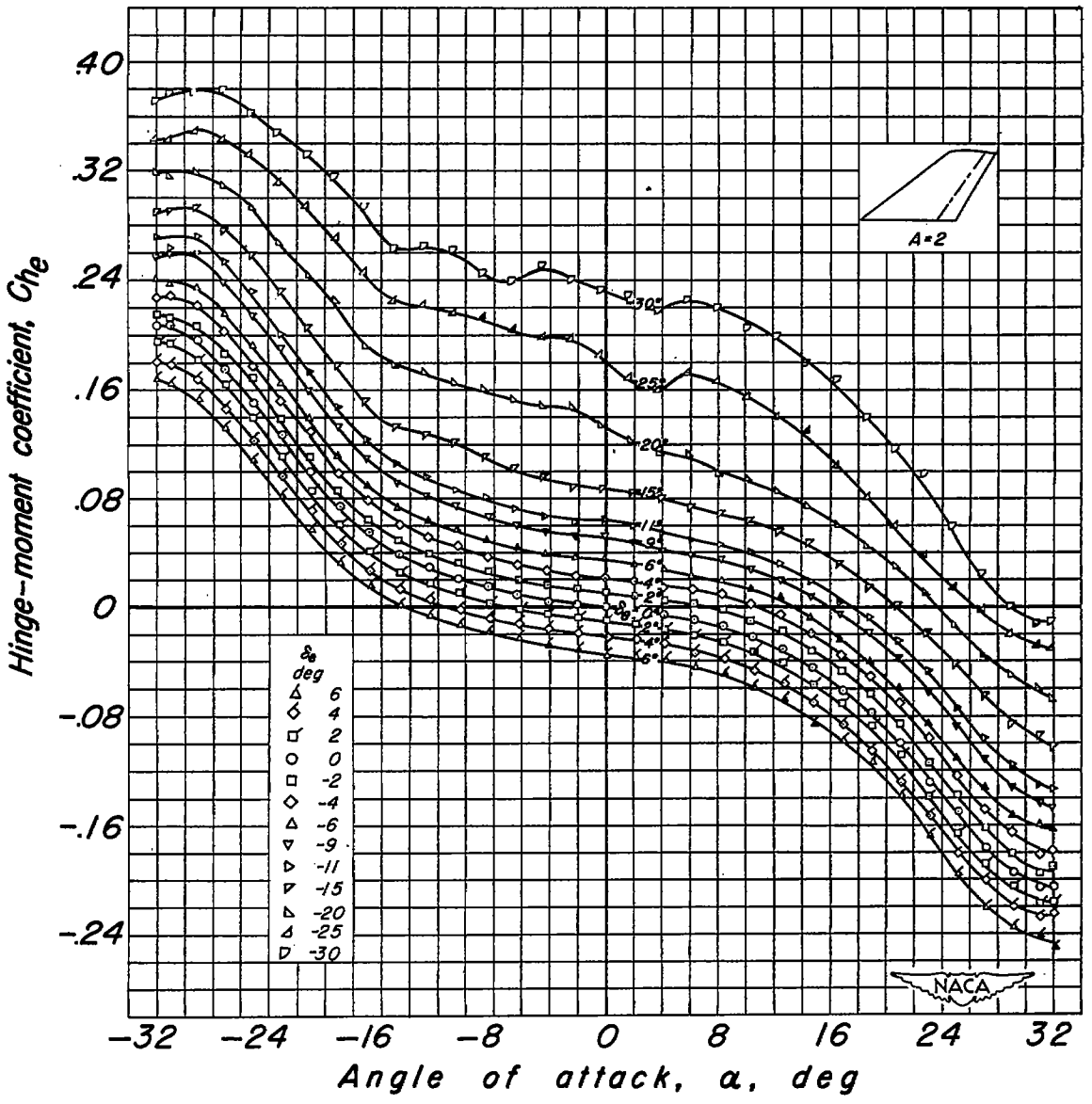

(b) Hinge-moment coefficient, C_{h_e}.

Figure 3.- Continued.

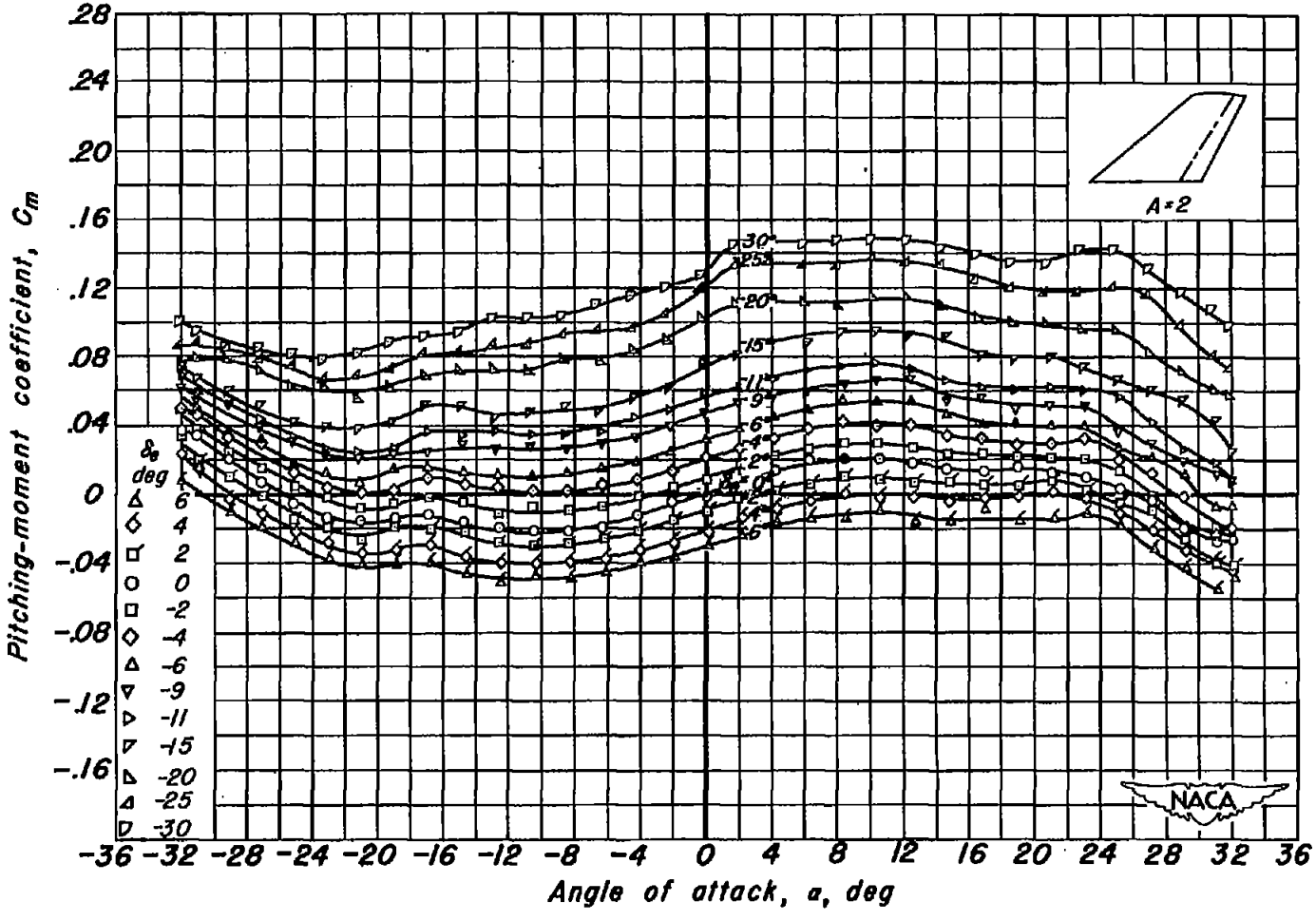

(c) Pitching-moment coefficient.

Figure 3.– Concluded.

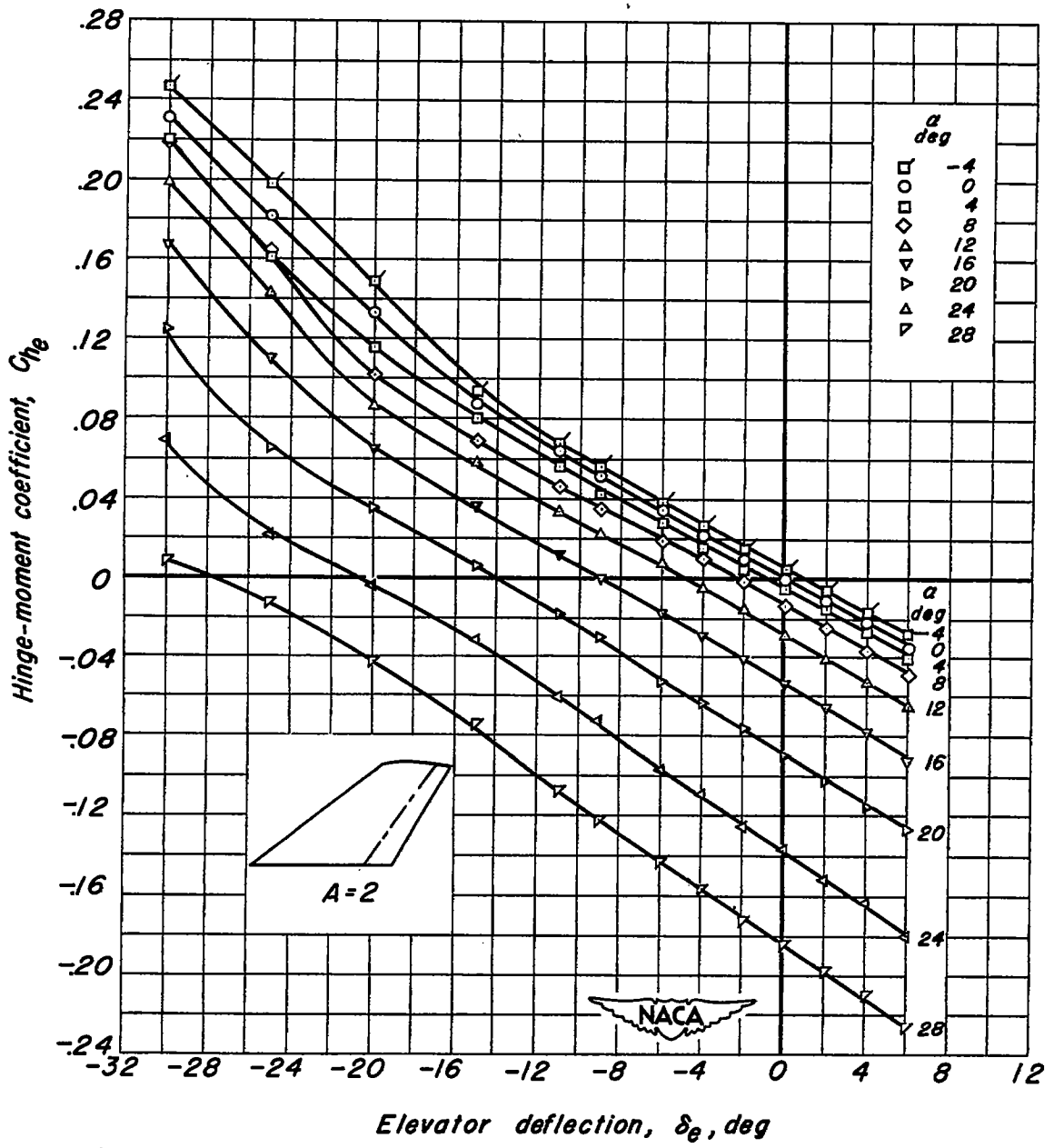

Figure 4.– Variation of hinge-moment coefficient with elevator deflection for various angles of attack for the 45° swept-back model of aspect ratio 2. R, 3.0×10^6.

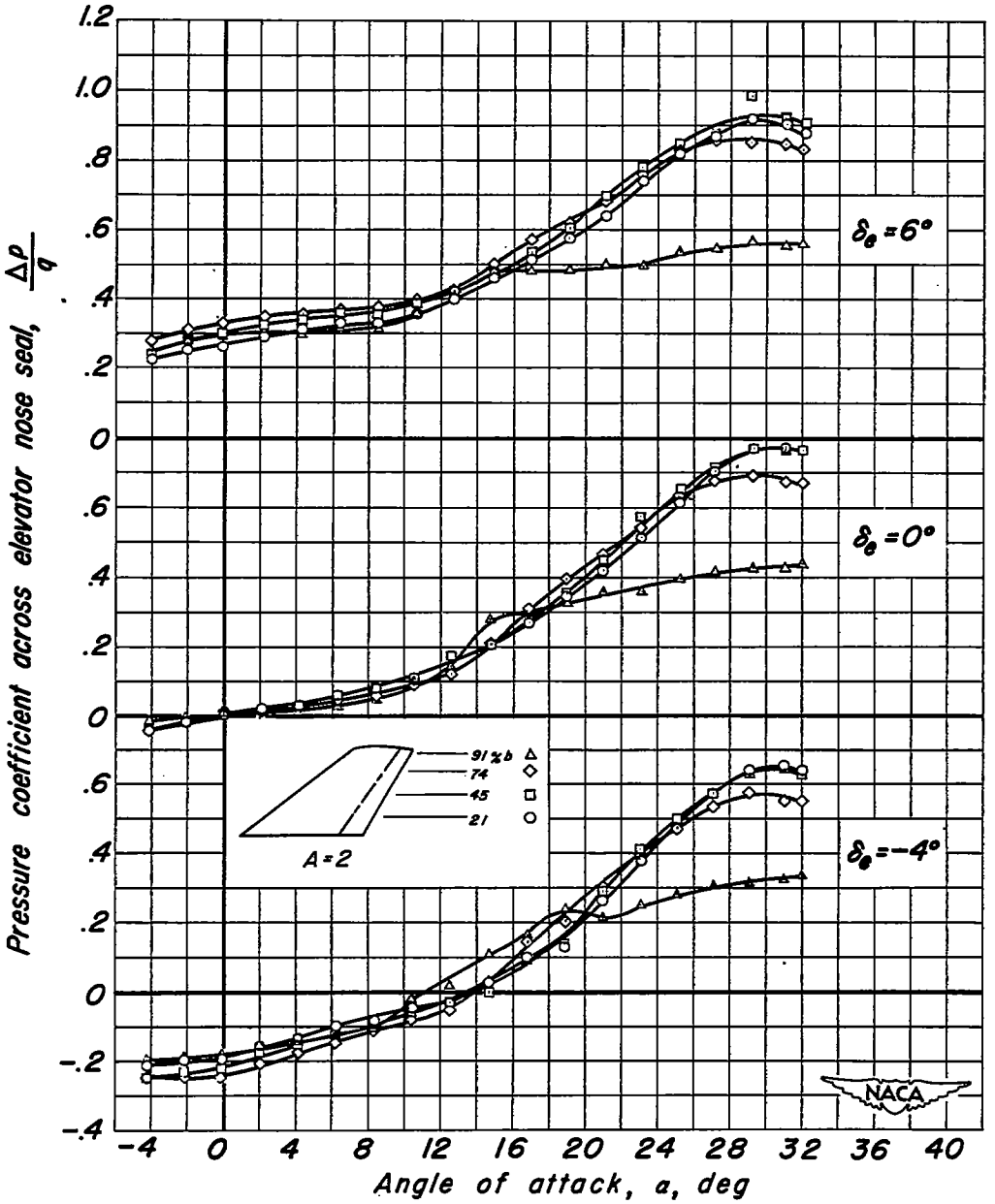

(a) $\delta_e = 6°, 0°, -4°$

Figure 5.– Variation of pressure coefficient across elevator nose seal with angle of attack for the 45° swept-back model of aspect ratio 2. R, 3.0×10^6.

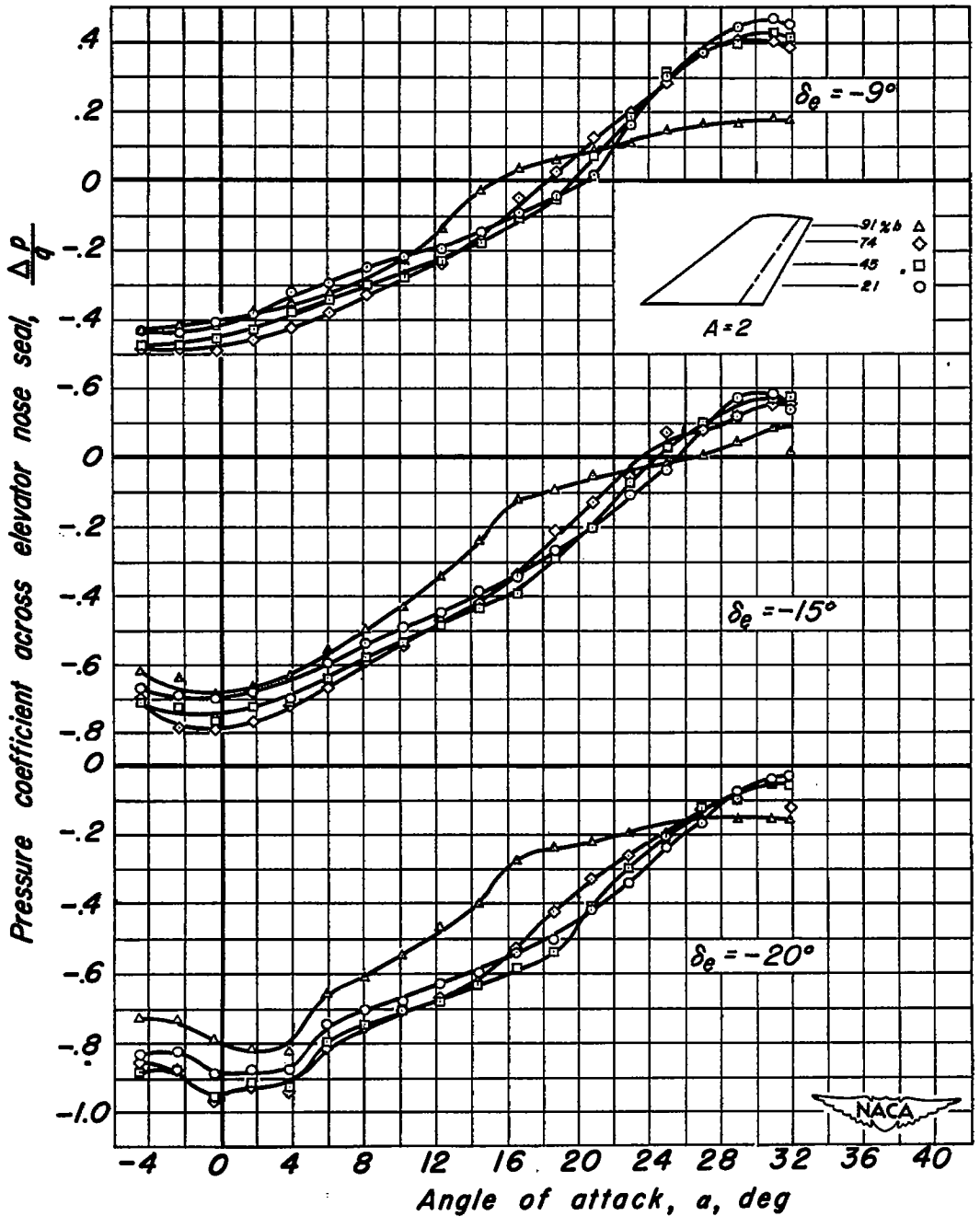

(b) $\delta_e = -9°, -15°, -20°$

Figure 5.—Concluded.

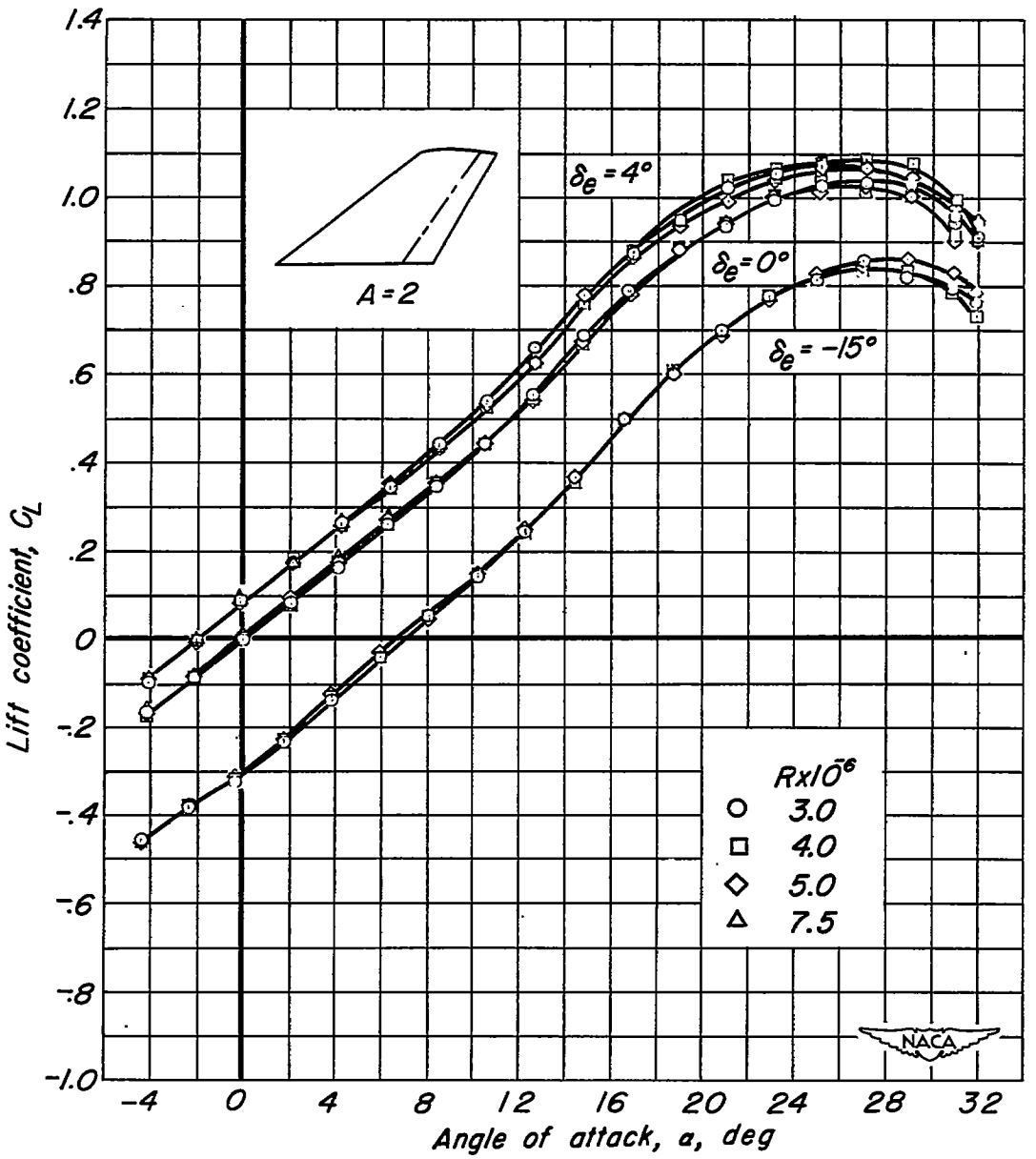

(a) Lift coefficient.

Figure 6.– Comparison of the lift and hinge-moment coefficients for various values of the Reynolds number for the 45° swept-back model of aspect ratio 2.

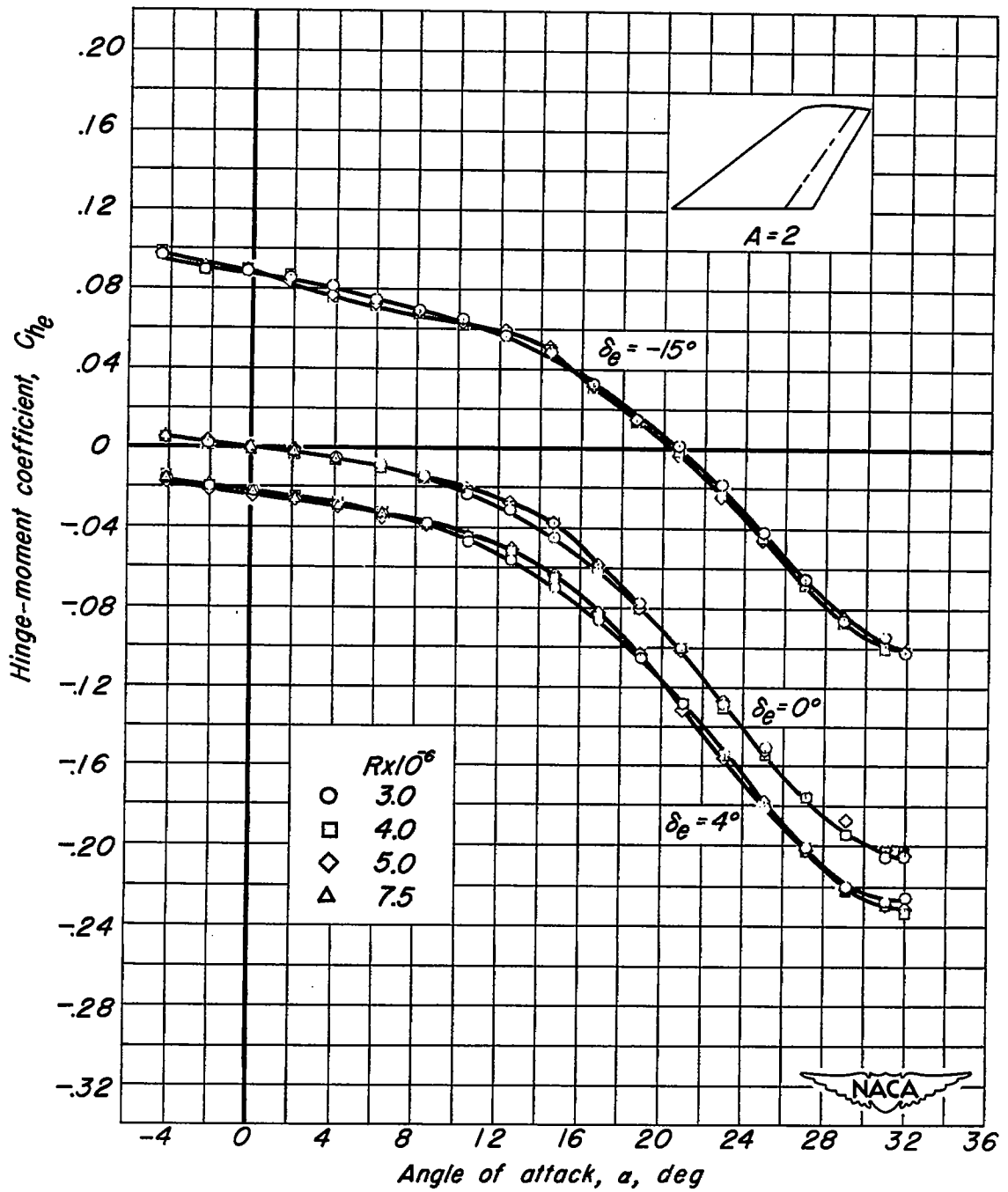

(b) Hinge-moment coefficient.

Figure 6.—Concluded.

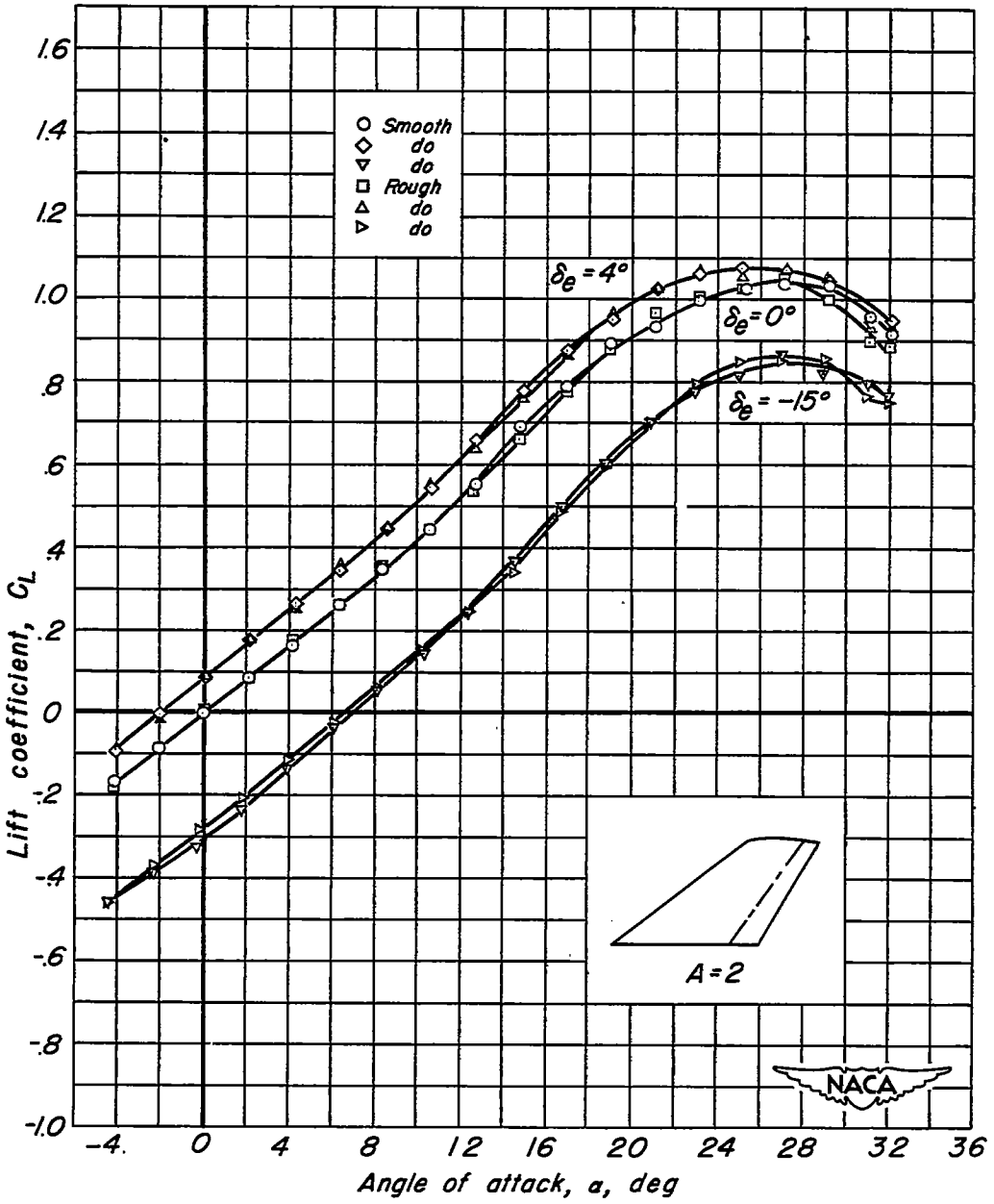

(a) Lift coefficient.

Figure 7.– Comparison of the lift and hinge-moment coefficients for the 45° swept-back model of aspect ratio 2, with and without leading-edge roughness. R, 3.0×10^6.

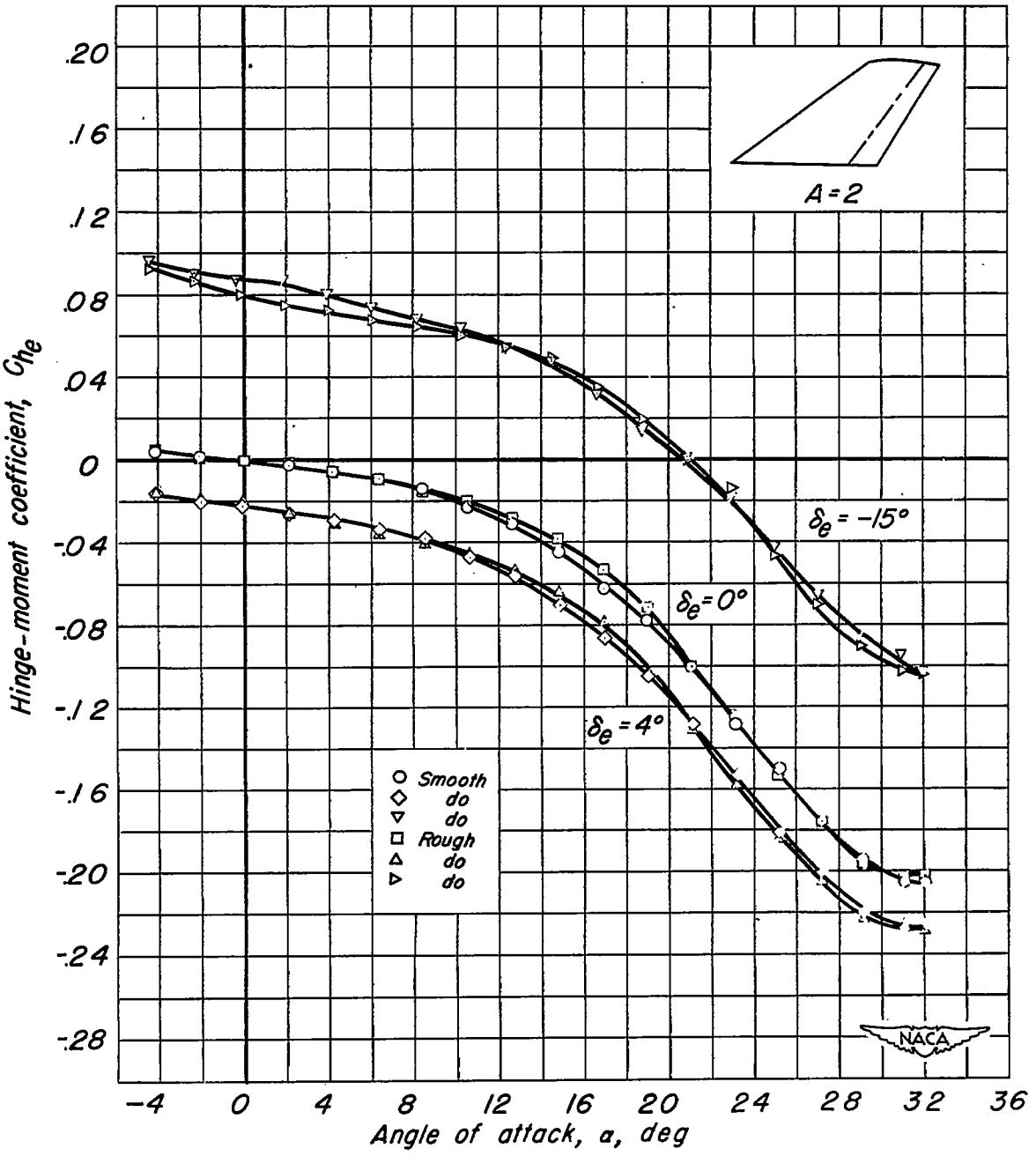

(b) Hinge-moment coefficient.

Figure 7.—Concluded.

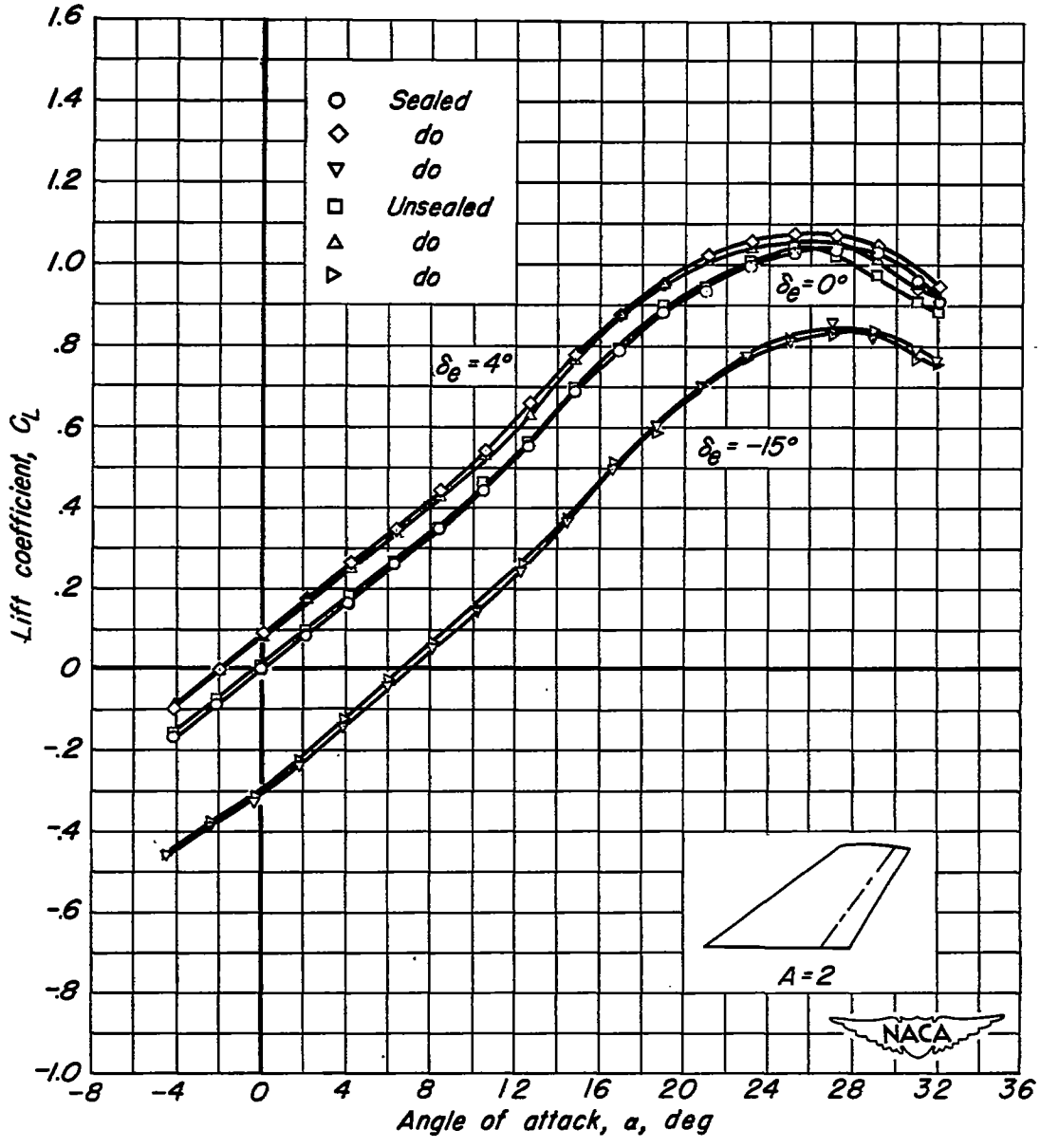

(a) Lift coefficient.

Figure 8.- Comparison of the lift and hinge-moment coefficients for the 45° swept-back model of aspect ratio 2, with and without elevator seal. R, 3.0×10^6.

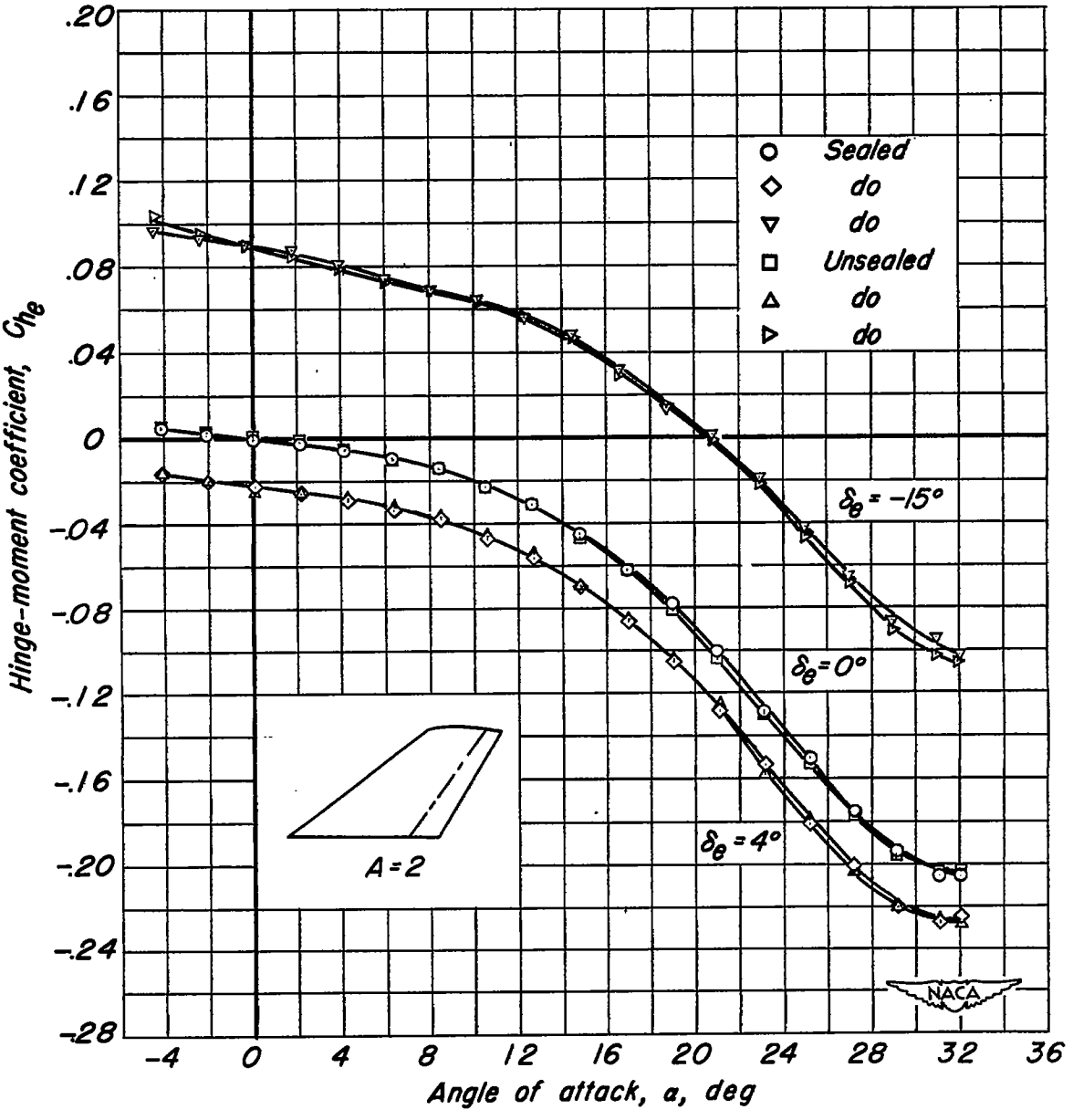

(b) Hinge-moment coefficient.

Figure 8.–Concluded.

(a) $\alpha = 0^{\circ}$, upper surface.

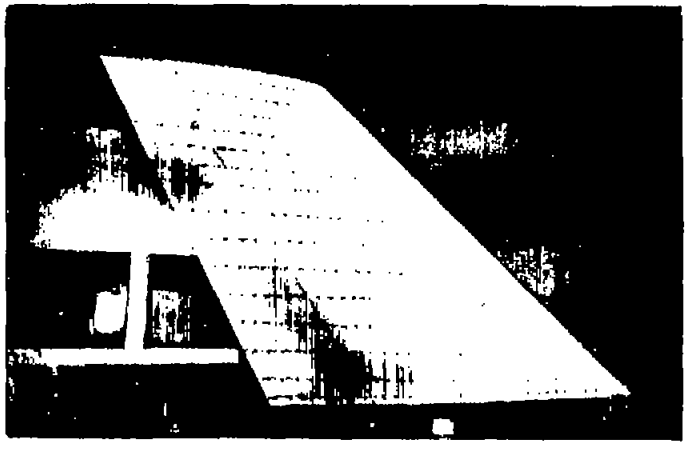

(b) $\alpha = 0^{\circ}$, lower surface.

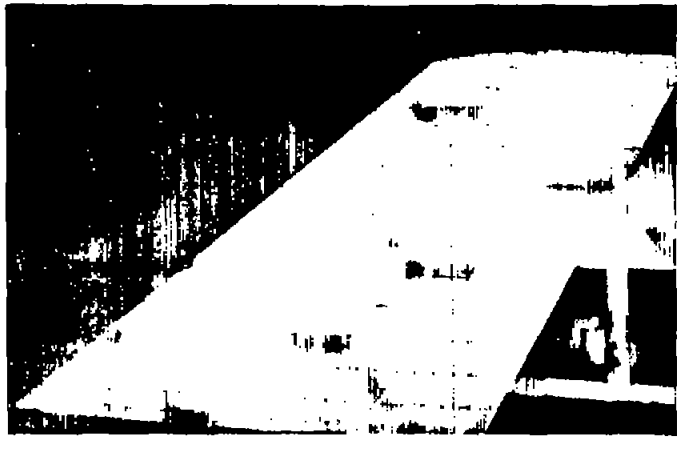

(c) $\alpha = 4.2^{\circ}$, upper surface.

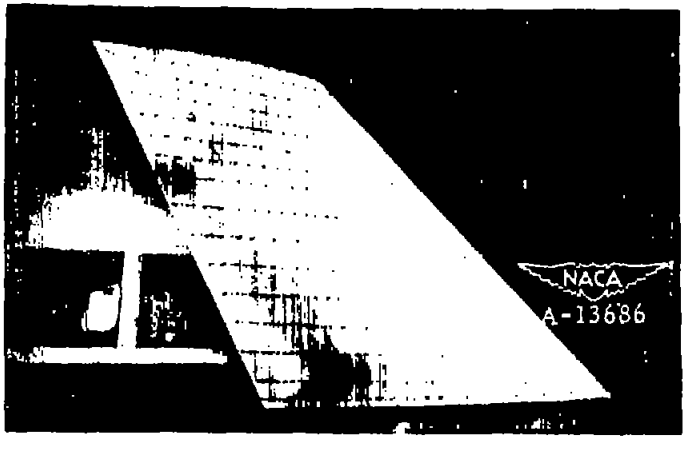

(d) $\alpha = 4.2^{\circ}$, lower surface.

Figure 9.– The air flow as indicated by tufts on the 45° swept-back model of aspect ratio 2 with the elevator undeflected. R, 3.0×10^{6}.

(e) $\alpha = 12.6^{\circ}$, upper surface.

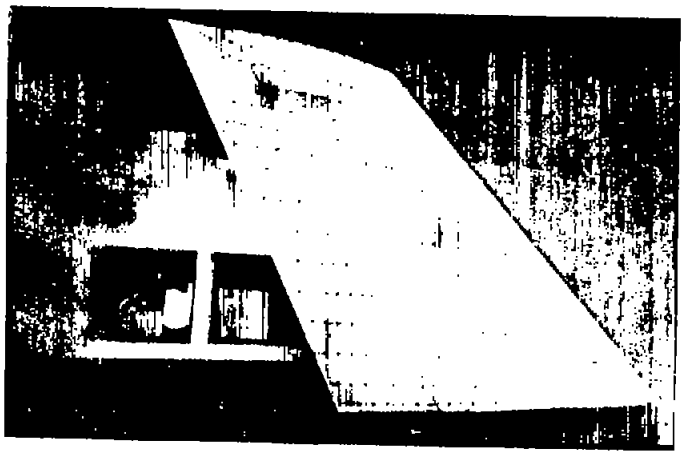

(f) $\alpha = 12.6^{\circ}$, lower surface.

(g) $\alpha = 16.9^{\circ}$, upper surface.

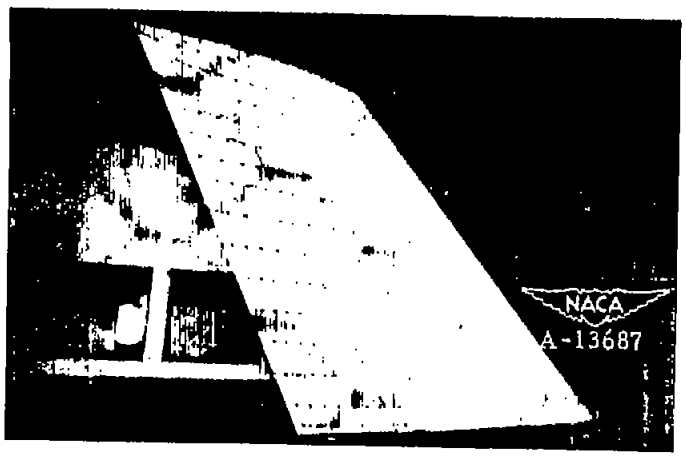

(h) $\alpha = 16.9^{\circ}$, lower surface.

Figure 9.- Continued.

(i) $\alpha = 21.0^{\circ}$, upper surface.

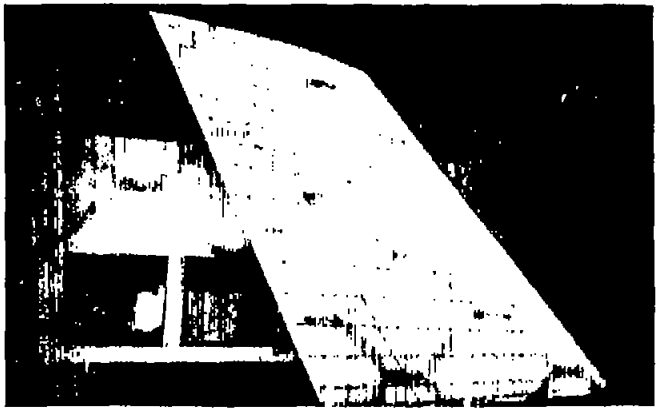

(j) $\alpha = 21.0^{\circ}$, lower surface.

(k) $\alpha = 25.2^{\circ}$, upper surface.

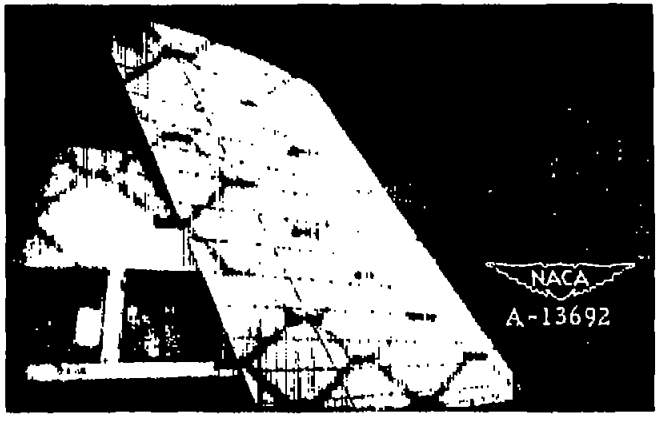

(l) $\alpha = 25.2^{\circ}$, lower surface.

Figure 9.– Continued.

(a) $\alpha = -0.3^{\circ}$, upper surface.

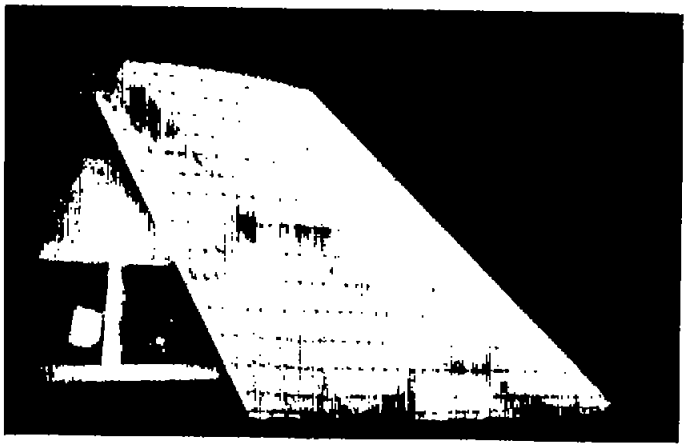

(b) $\alpha = -0.3^{\circ}$, lower surface.

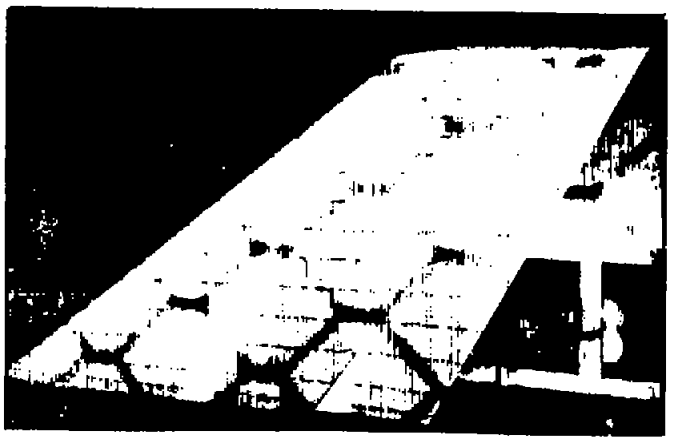

(c) $\alpha = 3.9^{\circ}$, upper surface

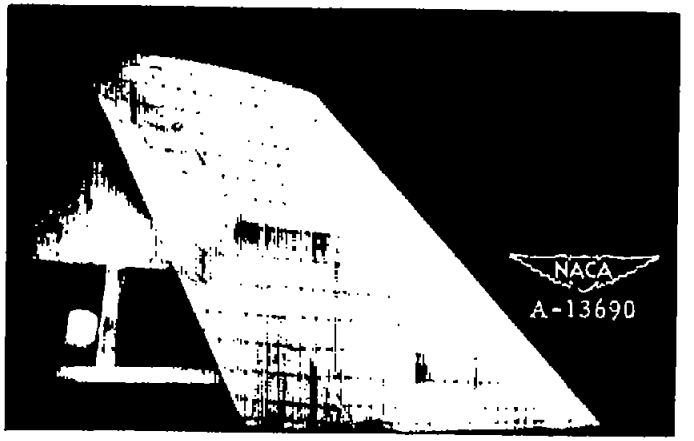

(d) $\alpha = 3.9^{\circ}$, lower surface.

Figure 10.- The air flow as indicated by tufts on the 45° swept-back model of aspect ratio 2 with the elevator deflected -15°. R, 3.0×10^{6}.

(e) $\alpha = 12.3^{\circ}$, upper surface.

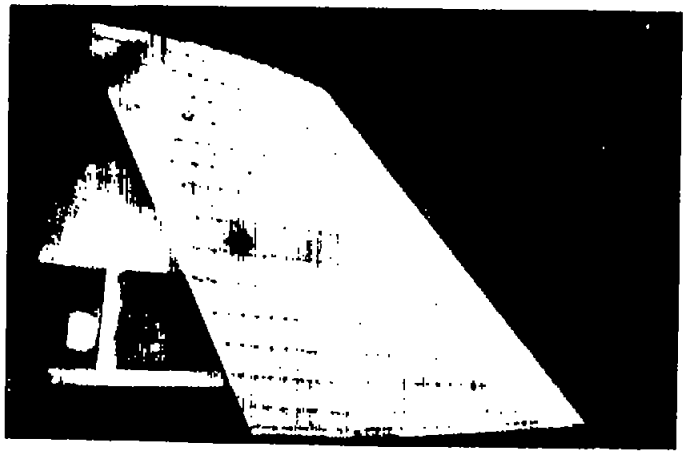

(f) $\alpha = 12.3^{\circ}$, lower surface.

(g) $\alpha = 16.6^{\circ}$, upper surface.

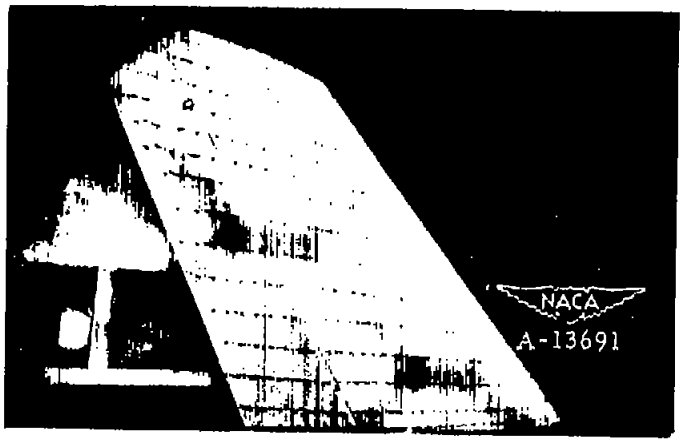

(h) $\alpha = 16.6^{\circ}$, lower surface.

Figure 10.– Continued.

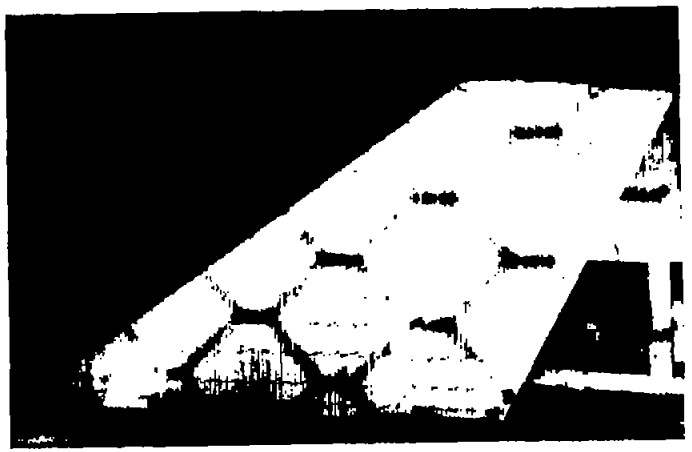

(i) $\alpha = 20.8^{\circ}$, upper surface.

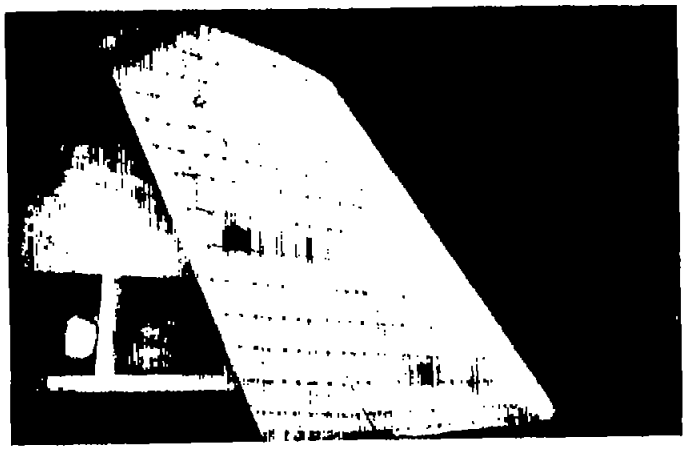

(j) $\alpha = 20.8^{\circ}$, lower surface.

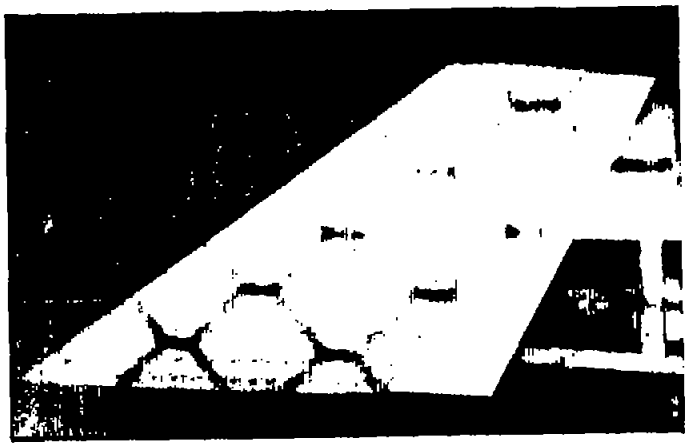

(k) $\alpha = 25.0^{\circ}$, upper surface.

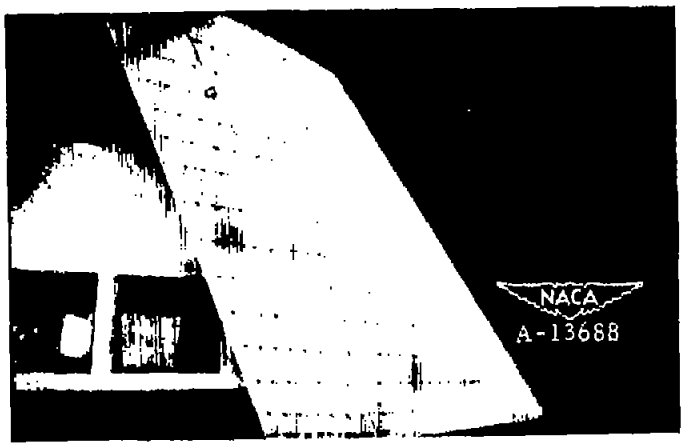

(l) $\alpha = 25.0^{\circ}$, lower surface.

Figure 10.— Continued.

(m) $\alpha = 28.9^{\circ}$, upper surface.

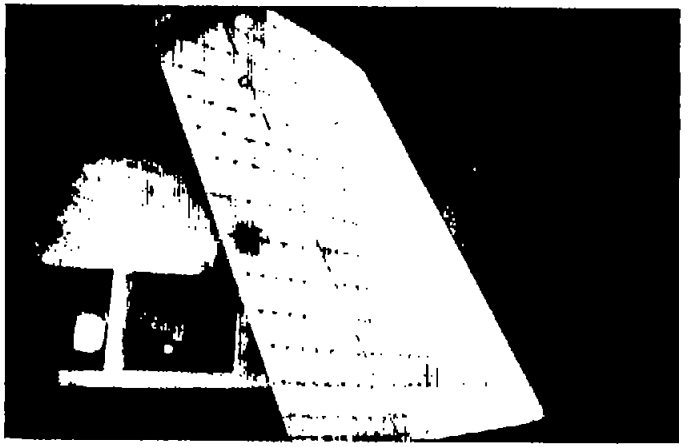

(n) $\alpha = 28.9^{\circ}$, lower surface.

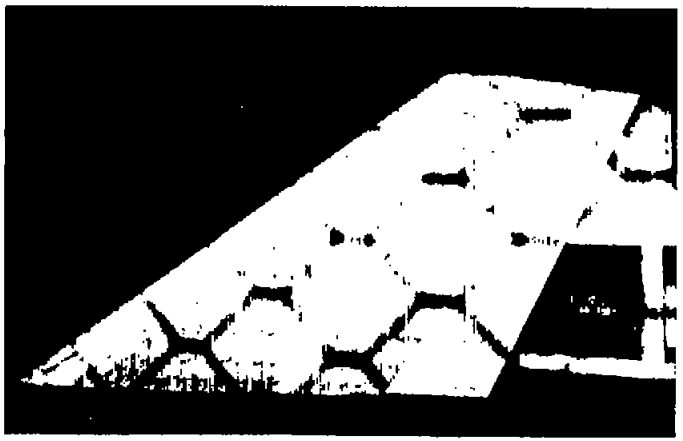

(o) $\alpha = 30.9^{\circ}$, upper surface.

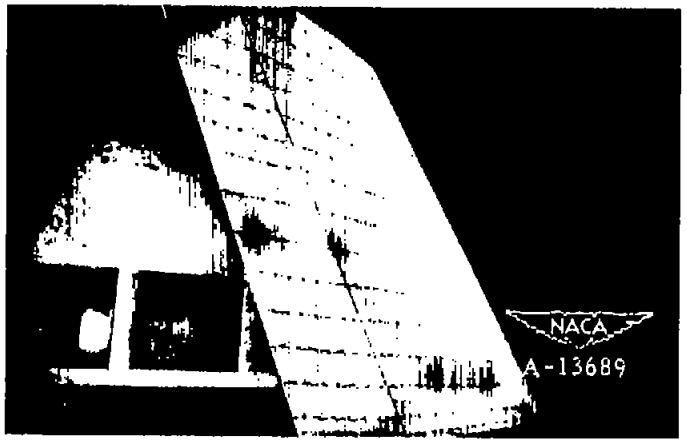

(p) $\alpha = 30.9^{\circ}$, lower surface.

Figure 10.– Concluded.